

Platinum-Coated Copper Nanowires with High Activity for Hydrogen Oxidation Reaction in Base

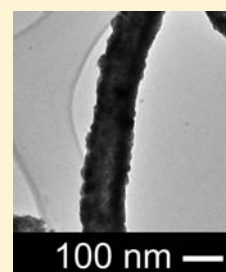
Shaun M. Alia,^{†,‡} Bryan S. Pivovar,[‡] and Yushan Yan^{*,†}

[†]Department of Chemical and Biomolecular Engineering, University of Delaware, Newark, Delaware 19716, United States

[‡]National Renewable Energy Laboratory, Golden, Colorado 80401, United States

S Supporting Information

ABSTRACT: Platinum (Pt)-coated copper (Cu) nanowires (Pt/CuNWs) are synthesized by the partial galvanic displacement of CuNWs and have a 100 nm diameter and are 25–40 μm length. Pt/CuNWs are studied as a hydrogen oxidation reaction (HOR) catalyst in base along with Cu templated Pt nanotubes (PtNT (Cu)), a 5% Cu monolayer on a bulk polycrystalline Pt electrode (5% ML Cu/BPPt), BPPt, and carbon supported Pt (Pt/C). Comparison of these catalysts demonstrates that the inclusion of Cu benefited the HOR activity of Pt/CuNWs likely by providing compressive strain on Pt; surface Cu further aids in hydroxyl adsorption, thereby improving the HOR activity of Pt/CuNWs. Pt/CuNWs exceed the area and mass exchange current densities of carbon supported Pt by 3.5 times and 1.9 times.



INTRODUCTION

Recently, polymer hydroxide exchange membrane fuel cells (HEMFCs) were developed as possible alternatives to polymer proton exchange membrane fuel cells (PEMFCs).^{1–5} The principal benefit of HEMFCs is their ability to avoid platinum group metal (PGM) catalysts.^{6–9} PEMFC kinetics is primarily limited by the oxygen reduction reaction (ORR) that requires an overpotential of about 300 mV for platinum (Pt) catalysts. Although a similar ORR overpotential has been observed in basic electrolytes, PGM catalysts are no longer essential.^{7,10,11} While Pt has similar ORR activity in base and acid, its hydrogen oxidation reaction (HOR) activity is at least 2 orders of magnitude slower in base.^{12–14} The development of HOR catalysts in base has primarily focused on PGMs, PGM alloys, and nickel.^{15–18} Significant achievements have been made in understanding HOR on Pt in base. Shao-Horn et al. determined the exchange current densities of HOR/hydrogen evolution reaction (HER) on carbon supported Pt (Pt/C) and a bulk polycrystalline Pt electrode (BPPt).¹⁴ Marković et al. examined low index Pt facets, finding that HOR activity increased in the order $(100) \leq (111) < (110)$.¹⁹ Marković et al. also studied the role of hydroxyl adsorption and suggested that the incorporation of oxophilic sites improved HOR/HER activity beyond pure Pt.²⁰ Yan et al. recently showed that HER/HOR activity in base can be correlated with hydrogen binding energy (HBE) via a volcano relationship, suggesting the importance of HBE.²¹ These results provide directions for designing and characterizing novel Pt catalysts for HOR in base.

Copper (Cu) templated Pt nanotubes (PtNTs (Cu)) and Pt-coated Cu nanowires (Pt/CuNWs) were recently investigated as ORR catalysts for PEMFCs, where the extended network, compressive strain, and preferentially exposed facets improved ORR activity.^{22–24} In this study, we explore similar materials for their ability to (1) improve Pt HOR mass and area activity by using Pt/CuNWs; (2) examine if the subsurface Cu

(represented by PtNT (Cu)) increases the HOR activity by lowering the HBE of Pt; and (3) examine if the presence of Cu on the catalyst surface (represented by a 5% ML Cu/BPPt) enhances the HOR activity by facilitating hydroxyl adsorption (schematic representations of catalysts presented in Figure 1). Pt/C was also included as a benchmark commercial catalyst for HOR mass activity.

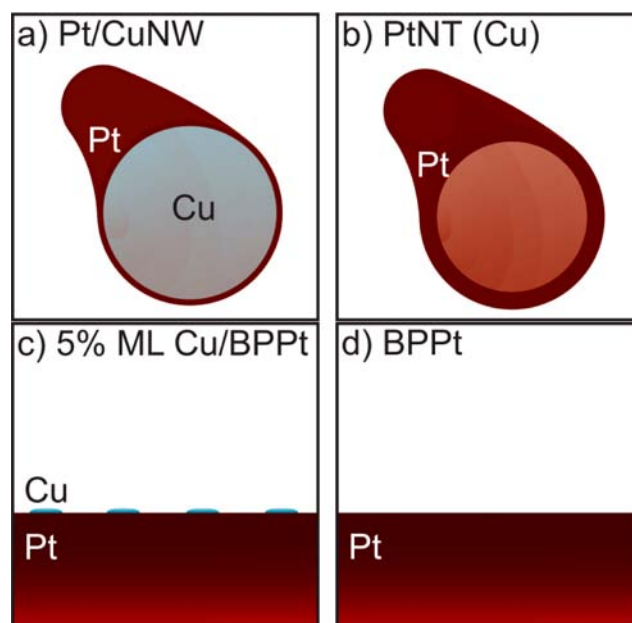


Figure 1. Schematic of (a) Pt/CuNWs, (b) PtNTs (Cu), (c) 5% ML Cu/BPPt, and (d) BPPt.

Received: June 4, 2013

Published: August 16, 2013

■ EXPERIMENTAL SECTION

CuNWs were synthesized by the reduction of Cu nitrate with hydrazine in sodium hydroxide.²⁵ An aqueous solution of Cu nitrate (0.188 g of Cu nitrate in 10 mL of water) was added to a 500 mL round-bottom flask containing chilled (~ 10 °C) 15 M sodium hydroxide (200 mL). The Cu nitrate solution was added slowly to prevent reduction; following addition, the flask was shaken vigorously to fully distribute the Cu nitrate. Solutions of as-purchased ethylene diamine (1.5 mL) and hydrazine (0.25 mL, 35 wt %) were then injected into the flask. The flask was capped and exposed to a 60 °C water bath for 1 h without stirring; following synthesis, the flask was cooled in an ice bath until the flask contents reached ~ 10 °C. The CuNW solution was filtered and washed with copious amounts of water. Prior to drying, the filter with the collected CuNW sample was stored in a glovebox containing argon. The method used for CuNW synthesis was similar to previously published methods.²⁵ The method reported here deviated slightly in terms of cleaning and storage. Using filtration increased CuNW yield and did not appear to promote Cu oxidation; hydrazine was also not used during storage to ensure that Pt reduction occurred solely through galvanic displacement.

PtNTs (Cu) were synthesized by the complete galvanic displacement of CuNWs. An aqueous CuNW dispersion (8.4 mg of CuNW in 200 mL of water) was added to a 500 mL round-bottom flask under magnetic stirring. Following 15 min of flowing argon, a chloroplatinic acid solution (36.0 mg of chloroplatinic acid in 100 mL of water) was added dropwise over a 15 min period. The flask proceeded at room temperature for 1 h; the flask was then heated in a water bath to 40 °C for 30 min and subsequently cooled to room temperature prior to removal of the PtNTs (Cu). PtNTs (Cu) were washed in an aqueous 1 M hydrochloric acid solution and water and annealed (250 °C for 1 h in 5% hydrogen, balance nitrogen) prior to electrochemical testing. Pt/CuNWs were synthesized by the partial galvanic displacement of CuNWs. The synthesis procedure for Pt/CuNWs was identical to the PtNT (Cu) synthesis in terms of reaction timing and CuNW concentration. The chloroplatinic acid solution, however, was diluted (3.5 mg of chloroplatinic acid in 100 mL of water). Following galvanic displacement, Pt/CuNWs were washed in an aqueous 1 M hydrochloric acid solution and water. Pt/CuNWs were not annealed to prevent thermal alloying. The method of PtNT (Cu) synthesis reported here was similar to previously published methods.²⁶ Slight deviations were noted in reactant concentration, drop time, and synthesis temperature. It was anticipated that the diluted synthesis conditions and slower drop rate promoted templating of the CuNW growth directions and lattice spacing. An elevated temperature (40 °C) following synthesis was used to promote the complete deposition of Pt.

Scanning electron microscopy (SEM) images were taken with a Phillips XL-30 FEG microscope at 20 kV. Transmission electron microscopy (TEM) samples were prepared by pipetting samples onto holey carbon-coated Cu grids. TEM images were taken with a Phillips CM300 microscope at 300 kV. Selected area electron diffraction (SAED) patterns were taken at a camera length of 32.0 cm. Inductively coupled plasma mass spectrometry (ICP-MS) experiments were conducted with a Thermo Scientific iCAP Q. Catalyst compositions were determined by examining five concentrations calibrated to a blank and three standards. Each measurement was run three times with a standard deviation less than 2% and an elemental dwell time of 0.15 s. Compositions were calculated on the basis of the Pt to Cu ratio, assuming that these metals accounted for the total catalyst mass. X-ray diffraction (XRD) patterns were taken on a Bruker D8 Discover (40 kV and 35 mA) and collected in the 2θ range 15–90° over 60 min. XRD samples were prepared by pipetting and drying concentrated materials onto a glass slide, capped by polyvinyl pyrrolidone (to ensure adhesion).

Rotating disk electrode (RDE) experiments were performed in a three-electrode glass cell equipped with a glassy carbon working electrode (Pine Instruments), Pt wire counter electrode, and mercury/mercurous oxide reference electrode (Koslow Scientific). Electrochemical measurements were taken on a multichannel potentiostat

(Princeton Applied Research), and working electrode rotation during HOR experiments was controlled with a modulated speed rotator (Pine Instruments). The working electrode was coated with Pt/CuNWs or PtNTs (Cu) by pipetting 20 μL of an aqueous suspension (0.98 mg_{metal} in 0.75 mL of water, 0.25 mL of isopropanol); this deposition corresponded to a total metal loading (Pt Cu) of 100 $\mu\text{g}_{\text{metal}} \text{cm}^{-2}$. The working electrode was coated with Pt/C by pipetting 20 μL of an aqueous suspension (0.18 mg_{metal} in 0.75 mL of water, 0.25 mL of isopropanol); this deposition corresponded to a Pt loading of 18 $\mu\text{g-Pt} \text{cm}^{-2}$. The 100 $\mu\text{g}_{\text{metal}} \text{cm}^{-2}$ loading was used for Pt/CuNWs and PtNTs (Cu) to ensure that each catalyst reached a proper diffusion limited current during HOR experiments. The 18 $\mu\text{g}_{\text{metal}} \text{cm}^{-2}$ loading was used for Pt/C to ensure that the HOR activity did not reach the Nernstian diffusion limited overpotential. The Pt loading for the catalysts of highest interest (Pt/CuNWs and Pt/C) was similar (16 $\mu\text{g-Pt} \text{cm}^{-2}$ for Pt/CuNWs, 18 $\mu\text{g-Pt} \text{cm}^{-2}$ for Pt/C), ensuring an even comparison. Reference electrode measurements were converted to RHE during HOR/HER experiments on BPt; the potential at which the current crossed the axis (i.e., transitioned between HOR and HER) was taken as the RHE value of the mercury/mercurous oxide reference electrode. KOH electrolytes were also changed with regularity (every 30 min) to ensure purity and a consistent pH.

Cu deposition on BPt occurred in 0.1 M sulfuric acid containing 0.1 M copper sulfate; the Cu deposition cell contained a Pt mesh counter electrode and was connected by a 0.1 M sulfuric acid filled liquid junction to a reference beaker containing a RHE in 0.1 M sulfuric acid.^{27,28} Cu deposition occurred at a variable potential for 1 min; Cu coverages of 5%, 38%, 53%, 95%, and 164% were achieved at 0.326, 0.325, 0.324, 0.323, and 0.322 V vs RHE, respectively. With the potential held, the BPt was removed from the Cu deposition cell and rinsed in water under rotation at 1600 rpm. The BPt was then characterized in KOH with HOR and cyclic voltammogram experiments. Following characterization in base, the BPt was rinsed in water and held at the deposition potential prior to being submerged into the Cu stripping cell; the Cu stripping cell contained argon saturated 0.1 M sulfuric acid, a Pt mesh counter electrode, and a RHE reference electrode. Cu stripping was conducted by rotating the working electrode at 1600 rpm and anodically scanning from the deposition potential to 1.2 V vs RHE at 100 mV s^{-1} . Cyclic voltammograms were immediately repeated to ensure complete Cu removal during the initial voltammogram.

■ RESULTS AND DISCUSSION

CuNWs (diameter 100 nm, length of 40–50 μm) were synthesized as the catalyst template by the hydrazine reduction of Cu nitrate in sodium hydroxide (Figure 2e and f).²⁵ Pt/CuNWs (diameter 100 nm, length of 25–40 μm) were synthesized by the partial galvanic displacement of CuNWs (Figure 2a and b). PtNTs (Cu) (wall thickness 11 nm, outer diameter 100 nm, and length of 5–20 μm) were synthesized by the complete galvanic displacement of CuNWs (Figure 2c and d). The composition of Pt/CuNWs (16.0 ± 0.5 wt % Pt, 84.0 ± 0.5 wt % Cu) and PtNTs (Cu) (90.1 ± 3.7 wt % Pt, 9.9 ± 3.7 wt % Cu) was determined by ICP-MS. These values were confirmed by energy dispersive X-ray spectroscopy, where Pt/CuNWs contained 18 wt % Pt and PtNTs (Cu) contained 95 wt % Pt. High-resolution TEM images and SAED patterns further confirmed templating of the Cu nanowire growth directions and lattice spacing (Supporting Information Figure S.1). SAED patterns matched patterns previously published by Zeng et al. and confirmed single twinned growth in the $[1, \bar{1}, 0]$ direction.²⁵

RDE experiments were utilized to determine the electrochemically active surface areas (ECSAs) and HOR activities. The catalyst loadings in the RDE experiments were as follows: Pt/CuNWs 16 $\mu\text{g}_{\text{Pt}} \text{cm}^{-2}$ (100 $\mu\text{g}_{\text{metal}} \text{cm}^{-2}$); PtNTs (Cu) 90 $\mu\text{g}_{\text{Pt}} \text{cm}^{-2}$ (100 $\mu\text{g}_{\text{metal}} \text{cm}^{-2}$); and Pt/C 18 $\mu\text{g}_{\text{Pt}} \text{cm}^{-2}$. Pt/

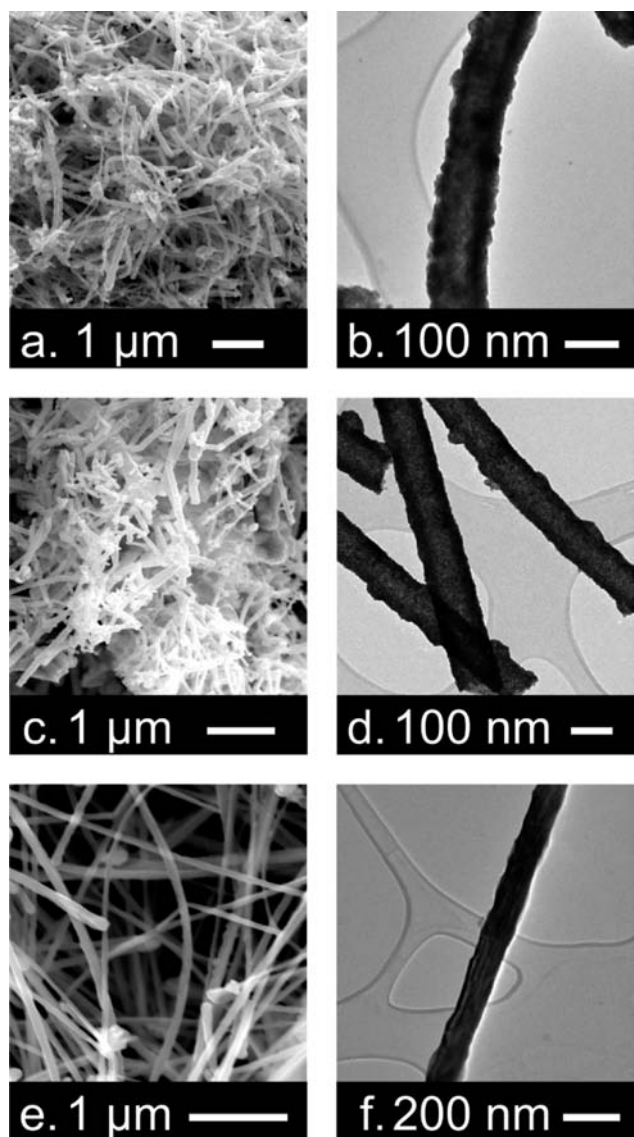


Figure 2. SEM and TEM images of (a,b) Pt/CuNWs, (c,d) PtNTs (Cu), and (e,f) CuNWs.

CuNWs and PtNTs (Cu) theoretically required a loading of 87.8 and 63.9 $\mu\text{g}_{\text{metal}} \text{cm}^{-2}$ to fully cover the working electrode. A loading of 100 $\mu\text{g}_{\text{metal}} \text{cm}^{-2}$ was utilized assuming partial nanotube/nanowire overlay (>10%) and was required to meet the diffusion limited current during HOR characterization. Pt/C was loaded to 18 $\mu\text{g}_{\text{Pt}} \text{cm}^{-2}$ because the higher loading caused the HOR activity to approach the Nernstian diffusion limited overpotential, invalidating the HOR characterization; the loading was chosen as similar to the Pt loading of Pt/CuNWs, providing a more ideal comparison. Assuming no overlay of the nanotubes/nanowires, Pt/CuNWs and PtNTs (Cu) had approximate catalyst layer thicknesses of 116.3 and 160.9 nm, respectively.

Pt ECSAs were determined from cyclic voltammograms in a 0.1 M KOH electrolyte by the charge associated with hydrogen adsorption, assuming a Coulombic charge of 210 $\mu\text{C} \text{cm}^{-2}$ (Supporting Information Figure S.2a). Pt/CuNWs, PtNTs (Cu), and Pt/C were found to have Pt ECSAs of 35.9, 5.9, and 59.6 $\text{m}^2 \text{g}_{\text{Pt}}^{-1}$, respectively. Pt/CuNWs had a Pt ECSA 6.1 times greater than PtNTs (Cu), although significant differences were not observed in the surface morphology of these catalysts

(Supporting Information Figures S.1 and S.3). The inner Pt surface on PtNTs (Cu) was potentially inaccessible, reducing the Pt ECSA (theoretically 5.3 $\text{m}^2 \text{g}_{\text{Pt}}^{-1}$ on the outer surface or 9.4 $\text{m}^2 \text{g}_{\text{Pt}}^{-1}$ total). Surface impurities of Cu were also more prevalent on Pt/CuNWs. Partial removal of surface Cu potentially roughened the Pt surface electrochemically, increasing the Pt ECSA (theoretically 22.8 $\text{m}^2 \text{g}_{\text{Pt}}^{-1}$).

The cyclic voltammogram of Pt/CuNWs was slightly distorted in comparison to a typical Pt response; this was attributed to the presence of Cu and its high stability in the alkaline electrolyte. The Pt ECSA of Pt/CuNWs was consistent with carbon monoxide oxidation voltammograms, assuming a Coulombic charge of 420 $\mu\text{C} \text{cm}^{-2}$ (Supporting Information Figure S.2b). The broad carbon monoxide oxidation peaks observed were also attributed to the presence of Cu on the surface. The redox characteristics of Cu (Supporting Information Figures S.4 and S.5a), were noted as: the anodic response at 0.35 V was for OH adsorption; the anodic response at 0.5 V vs RHE was Cu oxidation ($\text{Cu} \rightarrow \text{Cu(I)}$); the anodic response at 0.9 V vs RHE was Cu oxidation ($\text{Cu} \rightarrow \text{Cu(II)}$ and $\text{Cu(I)} \rightarrow \text{Cu(II)}$); the cathodic response at 0.45 V vs RHE was from Cu reduction ($\text{Cu(II)} \rightarrow \text{Cu(I)}$); and the cathodic response at 0.2 V vs RHE was Cu reduction ($\text{Cu(I)} \rightarrow \text{Cu}$).²⁹ The Cu oxidation (I,II) and reduction (I,0) features were evident in the voltammogram of Pt/CuNWs (Supporting Information Figure S.5b). The Cu ECSA in Pt/CuNW was determined from the Coulombic charge associated with Cu oxidation ($\text{Cu} \rightarrow \text{Cu(I)}$), using the PtNT (Cu) cyclic voltammogram as a pure Pt reference (Supporting Information Figure S.5c). The Pt/CuNW and PtNT (Cu) cyclic voltammograms were adjusted so that the Pt double charge layer reached the x-axis; the PtNT (Cu) response was then multiplied (by 0.829) to match the hydrogen desorption peak of Pt/CuNWs. The differences in the anodic current responses in the range 0.48–0.6 V vs RHE were integrated and attributed to Cu oxidation ($\text{Cu} \rightarrow \text{Cu(I)}$). The Coulombic charge was normalized to that obtained from bulk polycrystalline Cu (BPCu), where Cu oxidation ($\text{Cu} \rightarrow \text{Cu(I)}$) produced a Coulombic charge of 288.4 $\mu\text{C} \text{cm}^{-2}$, assuming no surface roughness (Supporting Information Figure S.5a). Through the Cu oxidation ($\text{Cu} \rightarrow \text{Cu(I)}$) current, Cu accounted for 6.8% of the Pt/CuNW surface, or an additional 0.4 $\text{m}^2 \text{g}_{\text{metal}}^{-1}$. The percentage of surface Cu content was determined from the Cu ECSAs and the Pt ECSAs as calculated by hydrogen underpotential deposition. In the case of Pt/CuNWs, the Pt-hydrogen adsorption response incorporated charges associated with Cu reduction ($\text{Cu(II)} \rightarrow \text{Cu(I)}$ and $\text{Cu(I)} \rightarrow \text{Cu}$). The Cu charge response did not affect the net calculated Pt ECSA because Cu reduction ($\text{Cu(II)} \rightarrow \text{Cu(I)}$) lowered the Pt double charging layer, decreasing the calculated Pt ECSA; and Cu reduction ($\text{Cu(I)} \rightarrow \text{Cu}$) contributed to the Pt hydrogen underpotential deposition charge, increasing the Pt ECSA. Carbon monoxide oxidation voltammograms also gave an identical Pt ECSA, confirming that surface Cu did not significantly impact the net Pt ECSA as calculated by Pt hydrogen underpotential deposition. The validity of the Cu ECSA method employed was further examined using BPpT covered with submonolayers of electrochemically deposited Cu. Cu ECSAs derived by alkaline cyclic voltammograms matched those obtained by acidic Cu stripping voltammograms in the range of 5–53% Cu coverage (Supporting Information Figures S.6–8). Cu ECSAs determined by Cu stripping voltammograms were calculated assuming a Coulombic charge of 420 $\mu\text{C} \text{cm}^{-2}$.^{27,28} Pt/CuNW

electrodes were further cycled in 0.1 M sulfuric acid to remove surface Cu; subsequent cyclic voltammograms in 0.1 M KOH yielded a Pt ECSA increase of 7.1% (indicating an initial Cu surface composition of 7.1% assuming a 1:1 relationship between removed Cu and exposed Pt).

Catalysts were evaluated for HOR during anodic linear polarization scans at 1600 rpm and 10 mV s^{-1} in a hydrogen saturated 0.1 M KOH electrolyte. HOR and HER activities were corrected for internal resistance (iR) by impedance spectroscopy measurements (10 kHz to 0.1 mHz) and hydrogen mass transport by the Koutecky–Levich equation (HOR portion); the kinetic activities (denoted i_k in Figure 3

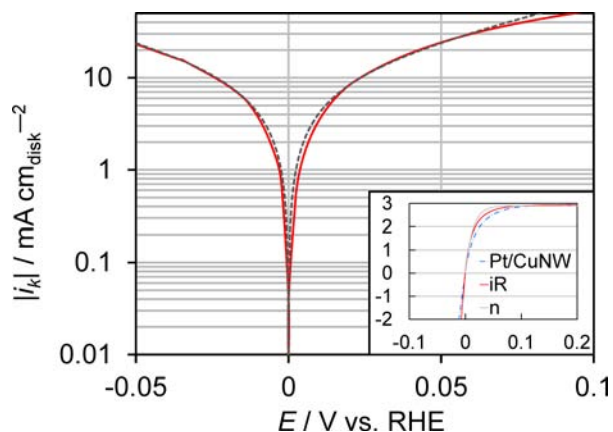


Figure 3. iR and mass transport corrected (—) HOR/HER activity of Pt/CuNWs in conjunction with the activity fitted to the Butler–Volmer equation (---) at 1600 rpm in a hydrogen saturated 0.1 M KOH electrolyte. Figure inset included the measured (---) and internal resistance corrected (—) linear polarization scans; the Nernstian diffusion limited overpotential was provided as a reference. Units for the inset axes mirror the main figures (x -axis E [V vs RHE], y -axis I [$\text{mA cm}_{\text{disk}}^{-2}$]).

and Supporting Information Figure S.9) were then fitted to the Butler–Volmer equation with $\alpha = 0.5$. Although RDE was inadequate to measure HOR in an acidic electrolyte, each catalyst failed to reach the Nernstian diffusion limited overpotential in the alkaline electrolyte, validating the HOR characterization.^{12,14} The similarity between the measured and fitted (Butler–Volmer equation) data was in agreement with the previous findings of Shao-Horn et al. and indicated that the HOR/HER kinetics followed the Tafel Volmer (rate limiting), Heyrovsky Volmer (rate limiting), or Heyrovsky (rate limiting) Volmer mechanisms.¹⁴ The Butler–Volmer fitting yielded HOR/HER exchange current densities (denoted i_0 in Figure 4) on a mass and area basis. The exchange current densities of Pt/C and BPt were in close agreement with those published by Shao-Horn et al.¹⁴ Pt/CuNWs produced area exchange current densities 3.5 times and 2.9 times that of Pt/C and BPt, respectively. On a PGM basis, Pt/CuNWs expressed an exchange current density 1.9 times that of Pt/C. Although PtNTs (Cu) also produced a high area exchange current density (2.8 times Pt/C, 2.3 times BPt), the Pt utilization was too low to match the mass exchange current density of Pt/C (25% of Pt/C).

The large exchange current density of Pt/CuNWs was partially attributed to electronic tuning. This is clearly illustrated by the PtNTs (Cu), which contained Cu but not surface Cu. In high-resolution TEM experiments, d -spacings

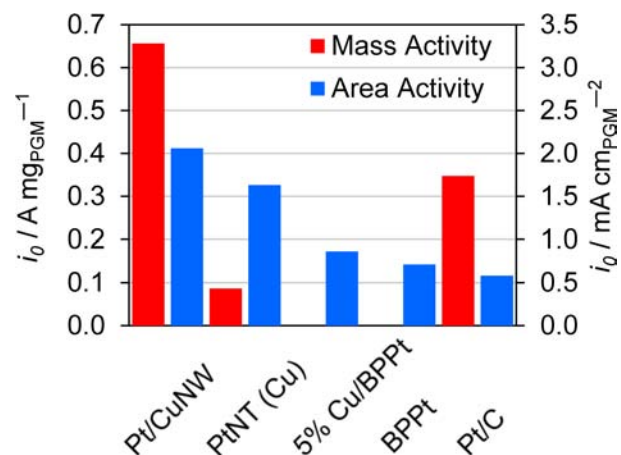


Figure 4. HOR mass and area normalized exchange current densities of Pt/CuNWs, PtNTs (Cu), 5% ML Cu/BPpt, BPpt, and Pt/C. Exchange current values were derived from Butler–Volmer fitting of HOR/HER data in the low overpotential region (-0.05 to $+0.05$ V vs RHE).

were observed between the $(1, \bar{1}, 1)$ lattice at 35.27° incident to the $(1, \bar{1}, 0)$ lattice (perpendicular to the dominant nanowire/nanotube growth direction, Supporting Information Figure S.1). Pt/CuNWs (0.212 nm) and PtNTs (Cu) (0.214 nm) were found to have a compressed $(1, \bar{1}, 1)$ spacing in comparison to pure Pt (0.226 nm), templated from the CuNWs (0.209 nm). XRD patterns further confirmed a compressed Pt lattice. Pt/CuNWs and PtNTs (Cu) were found to have lattice constants of 0.378 and 0.382 nm, compressed in comparison to Pt (0.392 nm, Supporting Information Figure S.10). The Pt lattice constants determined by XRD were slightly larger (3%) than those by SAED; SAED measurements potentially incorporated Cu, lowering the average lattice spacing relative to Pt zones.

Compressive strain (Supporting Information Figure S.1), introduced by the presence of Cu, widened the d-band and shifted the d-band center down relative to the Fermi level.^{30,31} The d-band shift weakened hydrogen chemisorption, thereby improving activity for HOR/HER.^{21,32,33} Previous studies further confirmed the d-band effect in Pt Cu binary systems.^{34–36} Norskov et al. calculated a negative d-band shift (-1.15 eV) for a Pt overlayer on Cu.³⁴ Strasser et al. studied Pt shell, Pt Cu core nanoparticles, finding that increasing Cu content increased strain, weakened oxygen chemisorption, and improved ORR activity.³⁵ Lou et al. examined Pt Cu nanocages, attributing an improvement in methanol oxidation activity to a Cu synergistic effect.^{37,38} Myles and Darby also studied Pt Cu alloys, finding that an increase in Cu content (up to 50–60%) filled the Pt d-band, thereby weakening bond strength.³⁶ Correlations between the d-band center and the HER activity of Pt were also indicative of HOR activity, because the Butler–Volmer equation equally fitted the HOR and HER portions (an increase in HER activity equally improved HOR).³³ The higher Cu content in the Pt/CuNWs may contribute to further tuning of the Pt d-band, potentially contributing to the improved HOR/HER area exchange current density in comparison to PtNTs (Cu).

The large exchange current density of Pt/CuNWs was also partially attributed to the presence of surface Cu creating catalyst bifunctionality. Marković et al. previously demonstrated that the addition of oxophilic sites (iridium or ruthenium)

improved HOR activity.²⁰ Norskov et al. have shown that Cu has oxygen and hydroxide binding energies similar to those of iridium and ruthenium.³⁹ Cu also initially oxidized at 0.35 V vs RHE (Supporting Information Figure S.4), a potential much lower than Pt (approximately 0.8 V vs RHE); although bulk electrochemical oxidation was not useful at the onset of HOR, it did experimentally indicate an increased oxophilicity in comparison to Pt.²⁹ To probe the effect of surface Cu on Pt HOR, submonolayers of Cu were electrochemically deposited onto BPt. Significant amounts of Cu ($\geq 38\%$ coverage) inhibited HOR activity, reducing both the exchange current density and the diffusion limited current (Supporting Information Figures S.11–13). This reduction was attributed to the inactivity of Cu in HOR (observed on BPCu, Supporting Information Figure S.11), primarily due to the weak Cu affinity to hydrogen chemisorption.³³ At a 5% Cu coverage, however, the Pt area exchange current density increased 27.5% above BPt; on an electrode area basis (mass activity equivalent), the exchange current density increased 21.1% above BPt. The increase in HOR activity confirmed the benefit of surface Cu and suggested a possible bifunctionality in the Pt/CuNW catalyst. Surface Cu provided adsorbed hydroxyl species, necessary in HOR, to proximate Pt sites.²⁰ While 5% coverage clearly showed improved performance, an optimum coverage between 0 and 38% was not determined.

Additionally, the templated growth directions and the presence of preferentially exposed facets and the extended surface were also considered as potential influences on HOR activity. Pt/CuNWs and PtNTs (Cu) maintained the $[1\bar{1}0]$ growth direction of the CuNWs. The surfaces available to participate in HOR/HER were primarily a combination of low and high index facets in the $\langle 110 \rangle$ zone axis.⁴⁰ Marković et al. previously found the (110) facet (largely unavailable to Pt/CuNWs, PtNTs (Cu)) to be the most active low index Pt facet for HOR; it therefore seemed unlikely that the Pt/CuNWs and PtNTs (Cu) benefitted significantly from the facets available.¹⁹ Previous studies further found a particle size effect for Pt in ORR, attributed to preferential activity on terrace sites.^{41–43} In contrast, little difference was observed in area exchange current densities of Pt/C and BPt, indicating a minimal particle size effect; it therefore seemed unlikely that extended network accounted for the large area exchange current densities of Pt/CuNWs and PtNTs (Cu).

Preliminary durability testing was completed on Pt/CuNWs and PtNTs (Cu) (100 mV s⁻¹, 0.05–1.2 V, 500 cycles, KOH electrolyte changed every 30 min) with no change observed in the Pt ECSA. Furthermore, Cu durability was seen as a minor concern in HOR as the diffusion limited current was reached at a potential (0.1 V vs RHE) far below Cu dissolution.

CONCLUSIONS

In summary, Pt/CuNWs, PtNTs (Cu), 5% ML Cu/BPpt, BPt, and Pt/C have been studied for HOR in base to investigate the effects of electronic tuning and hydroxyl adsorption; this study further demonstrates Pt/CuNWs as potentially a much superior HOR catalyst than Pt/C. Pt/CuNWs outperformed Pt/C in terms of area and mass exchange current densities by 3.5 times and 1.9 times, respectively. The increased activity observed on PtNT (Cu) and 5% ML Cu/BPpt over BPt clearly shows that the presence of Cu has a positive impact on HOR/HER. The observed improved performance seems to be largely driven by the electronic tuning provided by the Cu substrate and Cu

impurities within the Pt shell; however, the presence of Cu on the catalyst surface also appears helpful possibly by enhanced hydroxyl adsorption. The inclusion of Cu to increase the adsorption of hydroxyl species is potentially beneficial to a wide range of electrocatalysts. It is also likely that oxophilic materials other than Cu can be used to improve the HOR activity of Pt.

ASSOCIATED CONTENT

Supporting Information

Supplementary figures. This material is available free of charge via the Internet at <http://pubs.acs.org>.

AUTHOR INFORMATION

Corresponding Author

yanys@udel.edu

Notes

The authors declare no competing financial interest.

ACKNOWLEDGMENTS

Financial support is provided by the ARPA-E program of the U.S. Department of Energy.

REFERENCES

- (1) Varcoe, J. R.; Slade, R. C. T. *Fuel Cells* **2005**, *5*, 187.
- (2) Gu, S.; Cai, R.; Luo, T.; Chen, Z.; Sun, M.; Liu, Y.; He, G.; Yan, Y. *Angew. Chem., Int. Ed.* **2009**, *48*, 6499.
- (3) Gu, S.; Cai, R.; Luo, T.; Jensen, K.; Contreras, C.; Yan, Y. *ChemSusChem* **2010**, *3*, 555.
- (4) Kostalik, H. A.; Clark, T. J.; Robertson, N. J.; Mutolo, P. F.; Longo, J. M.; Abruna, H. D.; Coates, G. W. *Macromolecules* **2010**, *43*, 7147.
- (5) Wang, J. H.; Li, S. H.; Zhang, S. B. *Macromolecules* **2010**, *43*, 3890.
- (6) Spendelov, J. S.; Wieckowski, A. *Phys. Chem. Chem. Phys.* **2007**, *9*, 2654.
- (7) Wiberg, G. K. H.; Mayrhofer, K. J. J.; Arenz, M. *Fuel Cells* **2010**, *10*, 575.
- (8) Lu, S. F.; Pan, J.; Huang, A. B.; Zhuang, L.; Lu, J. T. *Proc. Natl. Acad. Sci. U.S.A.* **2008**, *105*, 20611.
- (9) Gu, S.; Sheng, W. C.; Cai, R.; Alia, S. M.; Song, S. Q.; Jensen, K. O.; Yan, Y. S. *Chem. Commun.* **2013**, *49*, 131.
- (10) Markovic, N. M.; Schmidt, T. J.; Stamenkovic, V.; Ross, P. N. *Fuel Cells* **2001**, *1*, 105.
- (11) Wu, G.; Chung, H. T.; Nelson, M.; Artyushkova, K.; More, K. L.; Johnston, C. M.; Zelenay, P. *ECS Trans.* **2011**, *41*, 1709.
- (12) Neyerlin, K. C.; Gu, W.; Jorne, J.; Gasteiger, H. A. *J. Electrochem. Soc.* **2007**, *154*, B631.
- (13) Bagotzky, V. S.; Osetrova, N. V. *J. Electroanal. Chem. Interfacial Electrochem.* **1973**, *43*, 233.
- (14) Sheng, W.; Gasteiger, H. A.; Shao-Horn, Y. *J. Electrochem. Soc.* **2010**, *157*, B1529.
- (15) Couturier, G.; Kirk, D. W.; Hyde, P. J.; Srinivasan, S. *Electrochim. Acta* **1987**, *32*, 995.
- (16) Tomantschger, K.; McClusky, F.; Oporto, L.; Reid, A.; Kordesch, K. *J. Power Sources* **1986**, *18*, 317.
- (17) Kirov, Y.; Schwartz, S. *J. Power Sources* **2000**, *87*, 101.
- (18) Shim, J.-P.; Park, Y.-S.; Lee, H.-K.; Lee, J.-S. *J. Power Sources* **1998**, *74*, 151.
- (19) Markovic, N. M.; Sarraf, S. T.; Gasteiger, H. A.; Ross, P. N. *J. Chem. Soc., Faraday Trans.* **1996**, *92*, 3719.
- (20) Strmcnik, D.; Uchimura, M.; Wang, C.; Subbaraman, R.; Danilovic, N.; van der, V.; Paulikas, A. P.; Stamenkovic, V. R.; Markovic, N. M. *Nat. Chem.* **2013**, *5*, 300.
- (21) Sheng, W.; Myint, M.; Chen, J.; Yan, Y. *Energy Environ. Sci.* **2013**, *6*, 1509.

- (22) Alia, S. M.; Zhang, G.; Kisailus, D.; Li, D.; Gu, S.; Jensen, K.; Yan, Y. *Adv. Funct. Mater.* **2010**, *20*, 3742.
- (23) Chen, Z.; Waje, M.; Li, W.; Yan, Y. *Angew. Chem., Int. Ed.* **2007**, *46*, 4060.
- (24) Alia, S. M.; Jensen, K.; Contreras, C.; Garzon, F.; Pivovar, B.; Yan, Y. *ACS Catal.* **2013**, *3*, 358.
- (25) Chang, Y.; Lye, M. L.; Zeng, H. C. *Langmuir* **2005**, *21*, 3746.
- (26) Lu, X.; McKiernan, M.; Peng, Z.; Lee, E. P.; Yang, H.; Xia, Y. *Sci. Adv. Mater.* **2010**, *2*, 413.
- (27) Green, C. L.; Kucernak, A. *J. Phys. Chem. B* **2002**, *106*, 1036.
- (28) Shyam, B.; Arruda, T. M.; Mukerjee, S.; Ramaker, D. E. *J. Phys. Chem. C* **2009**, *113*, 19713.
- (29) Pyun, C. H.; Park, S. M. *J. Electrochem. Soc.* **1986**, *133*, 2024.
- (30) Hammer, B.; Nørskov, J. K. *Nature* **1995**, *376*, 238.
- (31) Hammer, B.; Nørskov, J. K. In *Advances in Catalysis*; Bruce, C., Gates, H. K., Eds.; Academic Press: New York, 2000; Vol. 45, p 71.
- (32) Kitchin, J. R.; Nørskov, J. K.; Barteau, M. A.; Chen, J. G. *Phys. Rev. Lett.* **2004**, *93*, 156801.
- (33) Nørskov, J. K.; Bligaard, T.; Logadottir, A.; Kitchin, J. R.; Chen, J. G.; Pandelov, S.; Stimming, U. *J. Electrochem. Soc.* **2005**, *152*, J23.
- (34) Ruban, A.; Hammer, B.; Stoltze, P.; Skriver, H. L.; Nørskov, J. K. *J. Mol. Catal. A: Chem.* **1997**, *115*, 421.
- (35) Strasser, P.; Koh, S.; Anniyev, T.; Greeley, J.; More, K.; Yu, C.; Liu, Z.; Kaya, S.; Nordlund, D.; Ogasawara, H.; Toney, M. F.; Nilsson, A. *Nat. Chem.* **2010**, *2*, 454.
- (36) Myles, K. M.; Darby, J. B., Jr. *Acta Metall.* **1968**, *16*, 485.
- (37) Xia, B. Y.; Wu, H. B.; Wang, X.; Lou, X. W. *J. Am. Chem. Soc.* **2012**, *134*, 13934.
- (38) Xia, B. Y.; Ng, W. T.; Wu, H. B.; Wang, X.; Lou, X. W. *Angew. Chem.* **2012**, *124*, 7325.
- (39) Nørskov, J. K.; Rossmeisl, J.; Logadottir, A.; Lindqvist, L.; Kitchin, J. R.; Bligaard, T.; Jónsson, H. *J. Phys. Chem. B* **2004**, *108*, 17886.
- (40) Rathmell, A. R.; Bergin, S. M.; Hua, Y.-L.; Li, Z.-Y.; Wiley, B. J. *Adv. Mater.* **2010**, *22*, 3558.
- (41) Lee, S. W.; Chen, S.; Suntivich, J.; Sasaki, K.; Adzic, R. R.; Shao-Horn, Y. *J. Phys. Chem. Lett.* **2010**, *1*, 1316.
- (42) Mayrhofer, K. J. J.; Blizanac, B. B.; Arenz, M.; Stamenkovic, V. R.; Ross, P. N.; Markovic, N. M. *J. Phys. Chem. B* **2005**, *109*, 14433.
- (43) Geniès, L.; Faure, R.; Durand, R. *Electrochim. Acta* **1998**, *44*, 1317.